Using in situ Heating in the Transmission Electron Microscope to Probe the Retention of Implanted Solar Wind Gases Trapped in Bubbles in Dust Grains Exposed at the Surface of the Moon

Alexander M. Kling¹*, Kaitlyn Sycko¹, Beau S. Prince², Michelle S. Thompson¹, Zia Rahman³, Yao-Jen Chang², Thomas J. Zega^{2,4}

The solar wind, composed of ~96% hydrogen, ~4% helium, and <1% of other elements, implants high-energy (~1 keV/amu) ions into the surface of the Moon and other planetary bodies that lack atmospheres. This solar wind irradiation is a constituent process of space weathering, which over time, alters the chemical, microstructural, and spectral properties of the Moon and other airless bodies [1]. At the sub-micron scale, the cumulative effects of this solar wind irradiation on grains exposed at the surface of the Moon and airless bodies for thousands to millions of years includes the sputtering of atoms, the progressive disruption of the original crystalline structure, the development of complex defects such as vesicles (akin to bubbles), and the implantation of solar wind gases [2,3]. Advances in scanning transmission electron microscopy (STEM) and electron energy loss spectroscopy (EELS) capabilities have enabled the direct identification of solar wind-derived gases such as hydrogen, water, helium, and neon trapped in vesicles in space weathered lunar grains [3-5].

The retention of these solar wind-derived volatiles is of critical importance to understanding the mechanisms and timescales of the cycling of these species on the lunar surface. Micrometeoroid impacts, hypervelocity dust particles that constantly bombard the Moon, and the other dominant space weathering process, are proposed to be a major limit on the retention and lifetime of solar wind-derived species on the lunar surface. Here, we simulate the short-duration, high-temperature thermal conditions of a micrometeoroid impact on lunar dust grains within the transmission electron microscope and examine changes to the grains' microstructure, chemistry, and solar wind volatile contents.

Lunar grains were mounted on an aluminum scanning electron microscopy (SEM) stub coated in carbon tape and sputter-coated with carbon. Suitable grains of interest were identified using a Hitachi TM 4000 Plus benchtop SEM and a Quanta 3D FEG dual beam focused ion beam (FIB-SEM) at Purdue University. Cross-sections of these grains were extracted and thinned to electron transparency while preserving the top surface of the grain effected by solar wind irradiation using the Helios G4 UX dual beam FIB-SEM at Purdue University. These FIB sections were initially characterized for the presence of microstructural and chemical signatures of space weathering via transmission electron microscopy (TEM) using the Talos 200i and Themis Z STEMs at Purdue University. After initial characterization, we prepared these samples for in situ heating experiments by transferring them in situ within the FIB to microelectromechanical systems (MEMS) heating chips with supporting SiN films from Norcada []. This *in situ* transfer was

¹Department of Earth, Atmospheric, and Planetary Sciences, Purdue University, West Lafayette, IN, United States

²Lunar and Planetary Laboratory, University of Arizona, Tucson, AZ, United States

³Amentum, NASA Johnson Space Center, Houston, TX, United States

⁴Department of Materials Science and Engineering, University of Arizona, Tucson, AZ, United States

^{*} Corresponding Author: klinga@purdue.edu

performed using the Helios G4 UX FIB at Purdue University and the Quanta 3D FEG FIB at NASA Johnson Space Center.

Following the transfer of samples to the MEMS chips, we performed detailed TEM analyses and in situ heating experiments at the University of Arizona using the 200 keV aberrationcorrected Hitachi HF5000 S/TEM equipped with a Hitachi Blaze heating holder, bright-field, darkfield, and secondary electron detectors; dual Oxford 100 mm² windowless silicon-drift energy dispersive X-ray spectroscopy (EDS) detectors; and a Gatan Quantum Imaging Filter for EELS. Prior to heating, we performed high-resolution (HRTEM), bright-field (BF-STEM), dark-field (DF-STEM), and high-angle annular dark-field (HAADF-STEM) imaging to characterize the initial microstructure. We also performed EDS and EELS analyses to characterize the initial chemistry and presence of solar wind volatiles in the grain. EELS measurements were acquired over the low-loss energy region to search for the presence of solar wind-derived volatiles of interest such as water, hydrogen, helium, and neon. We also acquired core-loss EELS measurements of the Ti L_{2,3} edge, the O-K edge, and the Fe L_{2,3} edge to identify changes in the bonding environment or oxidation state as a result of heating. After these analyses, samples were heated to 1000°C and back to room temperature in 1 s to simulate the thermal effects of a micrometeoroid impact. After heating, we repeated the same imaging, EDS, and EELS measurements to characterize changes to the grain microstructure, chemistry, and presence and distribution of solar wind-derived species.

We have analyzed a lunar ilmenite; a Fe-Ti oxide mineral. Prior to heating, the lunar ilmenite grain displays a solar wind-damaged rim ~160 nm thick containing vesicles 3-10 nm in diameter, npFe particles, and vesicular npFe (vnpFe) particles. EELS analyses show that the vesicles and vnpFe particles contain helium via the presence of the He-K edge (Fig. 1). Following heating, we observe a series of chemical and microstructural changes that have implications on the mobilization and redistribution of solar wind implanted volatiles in lunar grains. The first change we observe is that many of the small (3-5 nm diameter) vesicles are no longer present and have been replaced by rounder, larger (up to ~40 nm diameter) vesicles (Fig. 2). These new vesicles likely formed from the diffusion and coalescence of precursor vesicles and defects during rapid heating. EELS analyses show that these new vesicles still contain helium and we observe a shift in the He-K to lower energies after heating relative to before heating, indicative of a decrease in the gas pressure within the vesicles (Fig. 2). This result demonstrating that helium may be retained in ilmenite during short-duration, high-temperature events such as a micrometeoroid impact.

We also observe the formation of new npFe particles and the growth and coalescence of preexisting npFe and vnpFe particles, likely due to Ostwald ripening [6]. The vnpFe particles have lost of their vesiculated textures, likely as a result of partial or complete melting and recrystallization, resulting in the loss of their helium contents. This result demonstrates a difference in the retention of helium for different known helium-carrying phases under conditions that may be experienced on the lunar surface. EELS spectra collected from the rim also reveal changes to the structure of the plasmon region following heating of the sample. After heating, there is an increase in the intensity of peaks at ~5.8, 11.6, 14.4, 39.4, and 47.6 eV. These peaks are associated with the TiO₆ octahedral bonding environment [7] and the increase in peak structure and intensity is likely indicative of defect annealing and atomic rearrangement during the rapid heating event. The annealing of defects would remove trapping sites for implanted helium, with the freed helium diffusing into vesicles or out of the grain altogether. The microstructural and chemical response of ilmenite and the redistribution of implanted helium during a simulated micrometeoroid impact may be extrapolated to other lunar materials and other implanted solar wind volatiles and future analyses will be performed on other lunar materials such as silicate minerals to test this hypothesis.

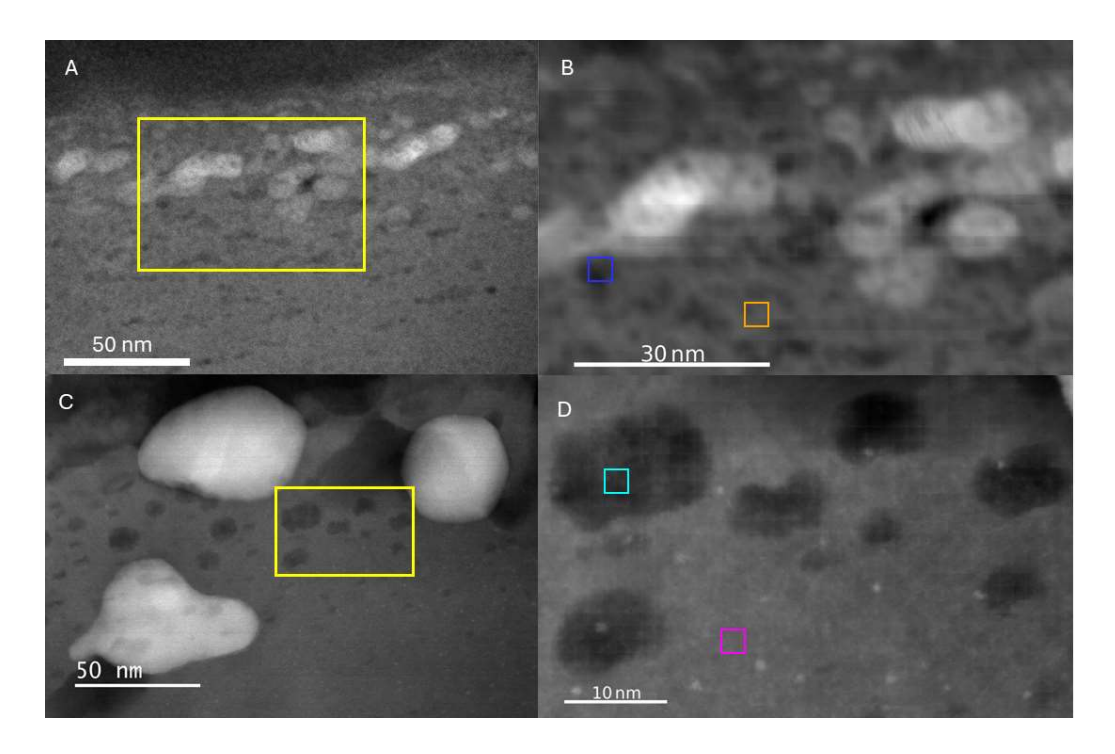


Figure 1. High-angle annular dark field (HAADF) scanning transmission electron microscopy images of the space weathered rim of the ilmenite before (A,B) and after (C,D) heating. Bright rounded objects are nanophase Fe particles and dark rounded objects are vesicles. The yellow box in A indicates the area of image B and the area of Figure 2A. The yellow box in Cindicates the area of image D and the area of Figure 2C. The orange, blue, cyan, and magenta boxes indicate summed pixels from which spectra in Figure 3 were acquired.

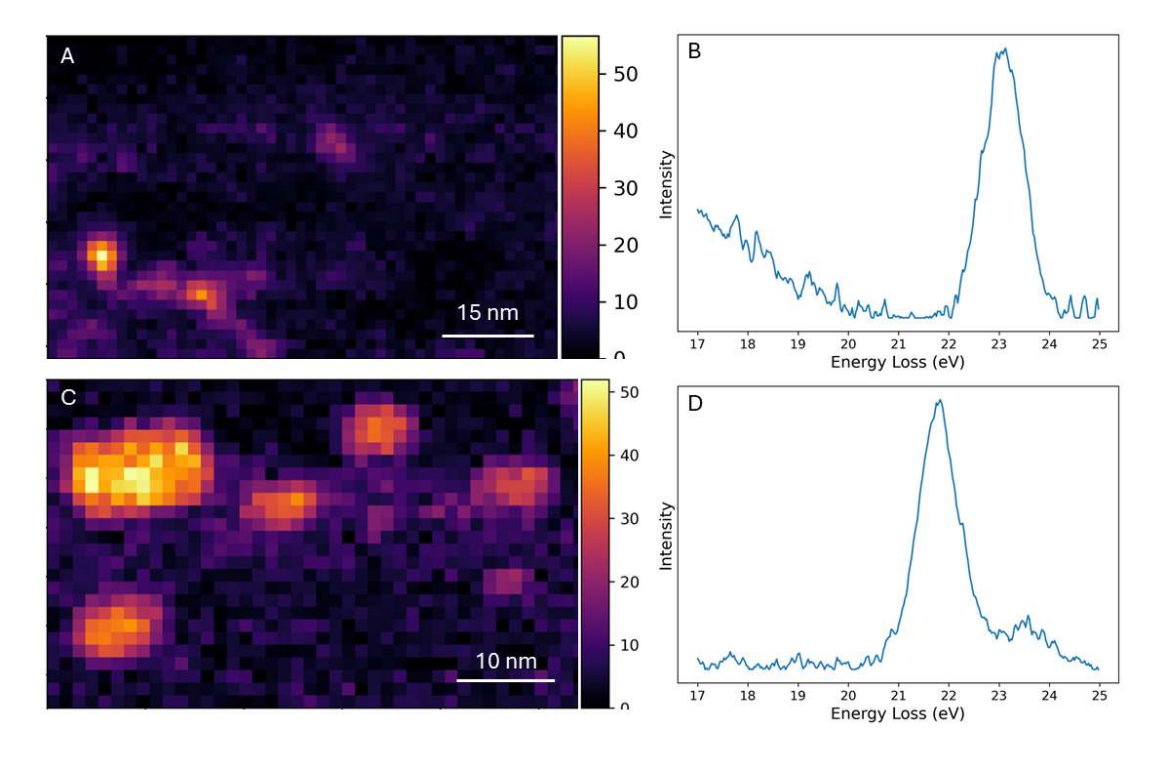


Figure 2. Maps and spectra of the helium K-edge (He-K) obtained via non-negative matrix factorization of the acquired spectrum images. A and B show the distribution and shape of the He-K edge before heating. C and D show the distribution and shape of the He-K edge after heating.

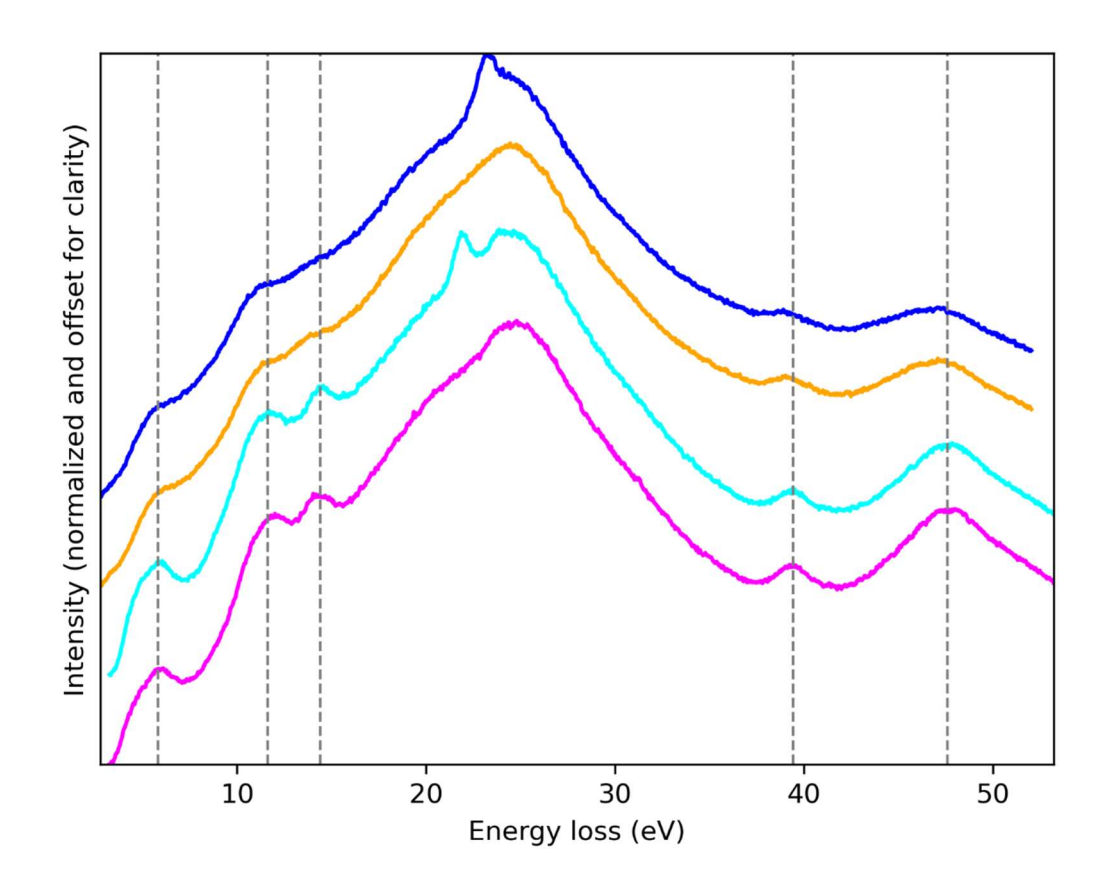


Figure 3. Electron energy loss spectra obtained from ilmenite rim material and within vesicles before and after heating. The spectra obtained after heating (cyan and magenta) have stronger peaks at ~5.8, 11.6, 14.4, 39.4, and 47.6 eV (dotted lines) relative to spectra obtained before heating (orange and blue).

References

- 1. Pieters, C. M. and Noble, S. K. *Journal of Geophysical Research: Planets* (2016) **121**(10), 1865–1884. https://doi.org/10.1002/2016JE005128
- 2. Keller, L. P. and McKay, D. S. Geochimica et Cosmochimica Acta (1997). 61, 2311–2341.
- 3. Kling, A. M. *et al. Earth and Planetary Science Letters* (2025) **651**, 119178. https://doi.org/10.1016/j.epsl.2024.119178
- 4. Cymes, B. A. *et al. Communications Earth & Environment* (2024). **5**(1), 1–8. https://doi.org/10.1038/s43247-024-01349-z
- 5. Kling, A. M., and Thompson, M. S. Lunar and Planetary Science Conference, 3040, 1567. (2024).

- 6. Thompson, M. S. *et al. Meteoritics and Planetary Science* (2017) **52**(3), 413–427. https://doi.org/10.1111/maps.12798
- 7. Bosman, M. *et al. Ultramicroscopy* (2006) **106**(11), 1024–1032. https://doi.org/10.1016/j.ultramic.2006.04.016
- 8. The authors acknowledge funding from NASA SSW grant 80NSSC20K0863 (MST) and NASA FINESST grant 80NSSC23K1368 (AMK). This work was enabled by the NFAR facilities at NASA Johnson Space Center and K-ALFAA facilities at the University of Arizona, both of which are supported under the NASA Planetary Science Enabling Facilities (PSEF) program.